RSC Advances

PAPER

View Article Online
View Journal | View Issue



Cite this: *RSC Adv.*, 2026, **16**, 19969

# Fluorine-engineered two-dimensional covalent organic frameworks for enhanced $C_2H_2/CO_2$ separation

Jialiang Liu,†[a] Wenjie Wei,†[a] Sen Wang,[a] Pengyue Hao,[a] Wang Zhang[a] and Yongwu Peng*[ab]

Received 10th February 2026
Accepted 11th April 2026

DOI: 10.1039/d6ra01174h

rsc.li/rsc-advances

Efficient separation of $C_2H_2$ from $CO_2$ remains a significant challenge owing to their closely matched molecular dimensions and physicochemical properties. Developing adsorbents capable of discriminating between these two gases is therefore of considerable importance for acetylene purification. Herein, we report two isoreticular two-dimensional covalent organic frameworks (COFs), TP-TFPB-COF and TP-NFPB-COF, featuring an hcb topology and constructed *via* [3 + 3] imine condensation. By increasing the fluorine content within the framework, TP-NFPB-COF exhibits enhanced $C_2H_2/CO_2$ separation performance, delivering an IAST selectivity of 2.86 at 298 K and 1 bar, compared with 2.04 for TP-TFPB-COF. Grand canonical Monte Carlo simulations reveal that the improved selectivity arises from increased pore polarity and strengthened C–H···F interactions with $C_2H_2$ molecules. This work highlights fluorination as an effective strategy for tuning pore environments and advancing COF-based acetylene separation.



## Introduction

Acetylene ($C_2H_2$) is an important light hydrocarbon feedstock extensively utilized in chemical synthesis and metal processing industries.[1,2] Industrial production of $C_2H_2$ typically relies on methane combustion or petroleum cracking, processes that inevitably introduce $CO_2$ as a major impurity.[3,4] The separation of $C_2H_2$ from $CO_2$ is particularly challenging because of their comparable kinetic diameters (~3.3 Å), linear geometries, and closely matched boiling points (189.2 K for $C_2H_2$ and 194.7 K for $CO_2$). Although cryogenic distillation is currently practiced, its high energy demand and associated carbon emissions motivate the exploration of alternative technologies.[5] Adsorptive separation based on porous solids has therefore attracted considerable attention owing to its lower energy consumption, operational flexibility, and potential for high selectivity.[7,8] A variety of porous adsorbents, including zeolites,[9] metal–organic frameworks (MOFs),[6,10–12] and porous organic polymers (POPs),[13,14] have been explored for gas separation applications.

More recently, covalent organic frameworks (COFs) have emerged as promising candidates owing to their high surface areas, ordered pore architectures, tailorable pore sizes, designable pore microenvironments, and excellent structural robustness.[15–21] Nevertheless, the application of COFs for $C_2H_2/CO_2$ separation remains at an early stage.[22–25] It is well established that functionalities such as unsaturated metal sites, Lewis basic moieties, and hydrogen-bond acceptors can significantly enhance gas separation performance.[26–29] Among them, fluorine substitution is particularly attractive: its high electronegativity not only improves framework hydrophobicity and thermal stability but also introduces unique electrostatic and hydrogen-bonding interactions, enabling fine regulation of pore microenvironments and strengthened host–guest affinity.[30–35]

Herein, we report two novel isoreticular two-dimensional (2D) COFs with hcb topology, namely TP-TFPB-COF and TP-NFPB-COF, constructed *via* [3 + 3] imine condensation of 2,4,6-trihydroxybenzene-1,3,5-tricarbaldehyde (Tp)[36–38] with two different $C_3$-symmetric fluorinated amines, 5′-(4-aminophenyl)-2′,4′,6′-trifluoro-[1,1′ : 3′,1″-terphenyl]-4,4″-diamine (TFPB) and 5′-(4-amino-3,5-difluorophenyl)-2′,3,3″,4′,5,5″,6′-heptafluoro-[1,1′ : 3′,1″-terphenyl]-4,4″-diamine (NFPB) (Scheme S1 and Fig. S1, SI). These COFs provide an ideal platform to elucidate the role of fluorination in $C_2H_2/CO_2$ separation. Notably, while both materials exhibit comparable $CO_2$ adsorption capacities, TP-NFPB-COF shows a markedly enhanced $C_2H_2$ uptake, resulting in superior $C_2H_2/CO_2$ separation performance. Grand canonical Monte Carlo (GCMC) simulations reveal that this improvement originates from strengthened host–guest interactions within the fluorine-rich pore microenvironment, where

[a]*College of Materials Science and Engineering, Science and Education Integration College of Energy and Carbon Neutralization, Zhejiang University of Technology, Hangzhou 310014, China. E-mail: ywpeng@zjut.edu.cn; pengyongwu@nbu.edu.cn*

[b]*School of Materials Science and Chemical Engineering, Ningbo University, Ningbo 315211, China*

† These authors contributed equally to this work.

multilayer and intralayer binding sites preferentially stabilize $C_2H_2$ molecules.

## Experimental section

### Synthesis of TP-TFPB-COF

TP-TFPB-COF were synthesized *via* a reversible [3 + 3] imine condensation reaction conducted at 120 °C for three days (Fig. 1 and Scheme S2, SI). A 10-mL Pyrex tube was charged with TP (12.6 mg, 0.06 mmol), TFPB (24.3 mg, 0.06 mmol) with DMA (0.4 mL) and BnOH (0.8 mL). The mixture was sonicated for 5 minutes to obtain a yellow turbid solution. To this, 9 M acetic acid (0.12 mL) were added as a catalyst. The tube was subsequently cooled to 77 K using a liquid nitrogen bath and subjected to three freeze–pump–thaw cycles for degassing. After sealing under vacuum, the tube was heated at 120 °C for 3 days. Upon cooling to room temperature, a yellow precipitate isolated by centrifugation at 40*g* (6000 rpm) for 2 minutes, washed with anhydrous acetone, and subjected to solvent exchange with anhydrous tetrahydrofuran three times. The sample was dried under vacuum at 80 °C 12 hours to yield a yellow powder.

### Synthesis of TP-NFPB-COF

TP-TFPB-COF were synthesized *via* a reversible [3 + 3] imine condensation reaction conducted at 120 °C for three days (Fig. 1 and Scheme S3, SI). A 10-mL Pyrex tube was charged with TP (12.6 mg, 0.06 mmol), NFPB (30.8 mg, 0.06 mmol) with mesitylene (0.5 mL) and 1,4-dioxane (0.5 mL). The mixture was sonicated for 5 minutes to obtain a yellow turbid solution. To this, 9 M acetic acid (0.1 mL) were added as a catalyst. The tube was subsequently cooled to 77 K using a liquid nitrogen bath and subjected to three freeze–pump–thaw cycles for degassing. After sealing under vacuum, the tube was heated at 120 °C for 3 days. Upon cooling to room temperature, a yellow precipitate was isolated through centrifugation at 40*g* (6000 rpm) for 2 minutes, washed with anhydrous acetone, and subjected to solvent exchange with anhydrous tetrahydrofuran three times. The sample was dried under vacuum at 80 °C 12 hours to yield a yellow powder.

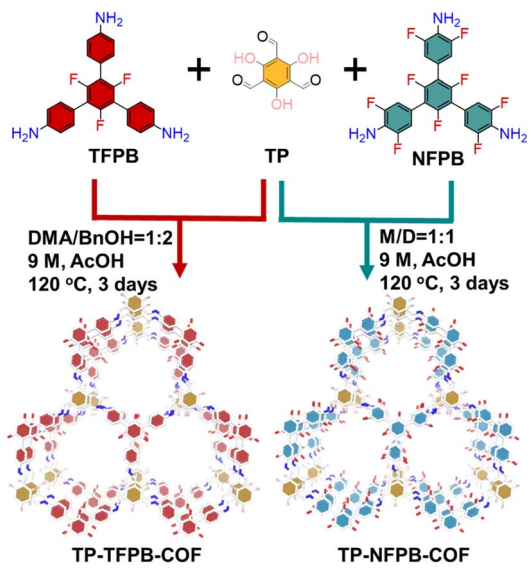


Fig. 1 Synthesis and structural diagrams of TP-TFPB-COF and TP-NFPB-COF.

## Results and discussion

### Characterization

Fourier-transform infrared (FT-IR) spectra confirm framework formation, showing characteristic C–N stretching vibrations at 1263 and 1280 $cm^{-1}$, and carbonyl stretching bands at 1623 and 1608 $cm^{-1}$ for TP-TFPB-COF and TP-NFPB-COF, respectively. The disappearance of aldehyde (1646 $cm^{-1}$) and amine (around 3400 $cm^{-1}$) signals from the precursors indicates near-quantitative conversion (Fig. S2 and S3, SI). Solid-state $^{13}C$ CP/MAS NMR spectra further corroborate the keto-enamine structures, with carbonyl resonances at 185.28 ppm for both COFs (Fig. S4 and S5, SI). Thermogravimetric analysis (TGA) demonstrates excellent thermal stability, with negligible weight loss below 450 °C under a nitrogen atmosphere (Fig. S6, SI). The chemical stability of both COFs was evaluated under various pH conditions, and PXRD patterns confirm the retention of crystallinity, indicating high pH stability[39] (Fig. S7, SI). Water contact angle measurements show that TP-NFPB-COF is superhydrophobic, exhibiting a contact angle of 151.0°, which is higher than that of TP-TFPB-COF (147.1°) (Fig. S8, SI). Scanning and transmission electron microscopy analyses reveal rod-like morphologies and high crystallinity, with clear lattice fringes observed in high-resolution TEM images (Fig. S9–S12, SI).

Powder X-ray diffraction (PXRD) patterns of both COFs exhibit sharp low-angle reflections, indicative of high crystallinity and identical framework topology (Fig. 2a and b).

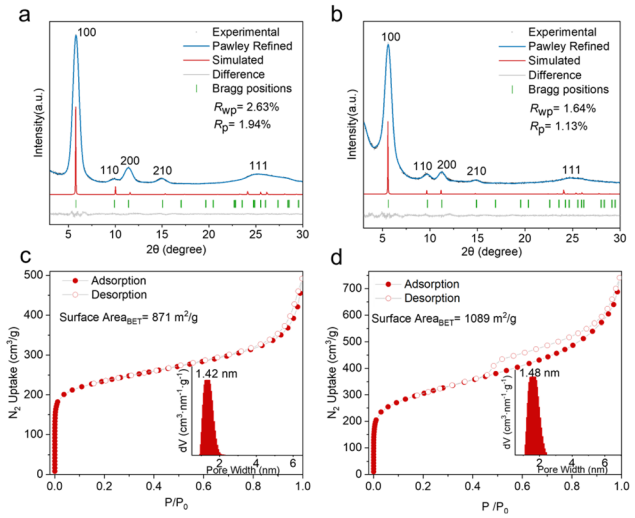


Fig. 2 (a and b) Experimental and refined PXRD patterns of (a) TP-TFPB-COF and (b) TP-NFPB-COF. (c and d) $N_2$ adsorption–desorption isotherms of (c) TP-TFPB-COF and (d) TP-NFPB-COF, with corresponding pore size distributions (insets).

Structural models based on eclipsed (AA), staggered (AB), and ABC stacking within the *P*3 space group were constructed (Fig. S13 and S14, SI). The experimental PXRD profiles closely match the simulated AA stacking model. TP-TFPB-COF displays reflections at 5.81°, 9.90°, 11.40°, 14.85°, and 25.09°, while TP-NFPB-COF shows corresponding peaks at 5.65°, 9.55°, 11.19°, 14.77°, and 24.85°, assignable to the (100), (110), (200), (210), and (111) planes. Pawley refinements afford low Rwp/Rp values (2.63%/1.94% for TP-TFPB-COF and 1.64%/1.13% for TP-NFPB-COF), validating the proposed structures (Tables S1 and S2, SI). The refined unit cell parameters are $a = b = 17.65$ Å, $c = 3.80$ Å for TP-TFPB-COF, and $a = b = 18.30$ Å, $c = 3.80$ Å for TP-NFPB-COF.

Nitrogen sorption measurements at 77 K reveal reversible type I isotherms for both COFs, indicative of their microporous characteristics (Fig. 2c and d). TP-TFPB-COF and TP-NFPB-COF exhibit maximum $N_2$ maximum uptakes of 492 and 727 $cm^3\ g^{-1}$, corresponding to BET surface areas of 871 and 1089 $m^2\ g^{-1}$, respectively. Non-local density functional theory (NLDFT) analysis shows narrow pore size distributions centered at 1.42 and 1.48 nm, in good agreement with theoretical values derived from structural models (Fig. 2c and d).

### $C_2H_2/CO_2$ adsorption and separation

The permanent porosity and fluorine-decorated pore environments of TP-TFPB-COF and TP-NFPB-COF prompted evaluation of their gas adsorption and separation performance. Single-component adsorption isotherms measured at 298 K show that both COFs preferentially adsorb $C_2H_2$ over $CO_2$ (Fig. 3). TP-TFPB-COF exhibits uptake capacities of 65.4 $cm^3\ g^{-1}$ for $C_2H_2$ and 47.9 $cm^3\ g^{-1}$ for $CO_2$, whereas TP-NFPB-COF shows enhanced $C_2H_2$ uptake (72.2 $cm^3\ g^{-1}$) accompanied by reduced $CO_2$ adsorption (39.8 $cm^3\ g^{-1}$). Both COFs retain substantial adsorption capacity over five cycles, demonstrating good recyclability (Fig. S15, SI).

To further understand the gas sorption behavior, the coverage-dependent adsorption enthalpies ($Q_{st}$) were calculated using the Clausius–Clapeyron equation. As shown in Fig. S16, TP-NFPB-COF exhibits a significantly higher zero-coverage $Q_{st}$ for $C_2H_2$ (28.5 kJ $mol^{-1}$) than for $CO_2$ (12.9 kJ $mol^{-1}$). In contrast, TP-TFPB-COF shows comparable $Q_{st}$ values for $C_2H_2$ (25.8 kJ $mol^{-1}$) and $CO_2$ (23.4 kJ $mol^{-1}$). These results indicate that the higher fluorine content in TP-NFPB-COF enhances the adsorption affinity toward $C_2H_2$, thereby amplifying the adsorption contrast between the two gases (Fig. 3a and b). To elucidate host–guest interactions at the molecular level, density functional theory (DFT) calculations were performed (Fig. S17, SI). TP-NFPB-COF exhibits stronger binding toward $C_2H_2$ ($E_{ads}$ = −0.172 eV) than $CO_2$ ($E_{ads}$ = −0.127 eV), and stronger $C_2H_2$ interaction than TP-TFPB-COF ($E_{ads}$ = −0.119 eV). In comparison, the adsorption energy of $CO_2$ on TP-TFPB-COF is −0.107 eV. These results confirm that enhanced fluorination strengthens host–guest interactions with $C_2H_2$, leading to improved selectivity.

Ideal adsorbed solution theory (IAST) calculations for equimolar $C_2H_2/CO_2$ mixtures at 298 K yield selectivities of 2.04 for TP-TFPB-COF and 2.86 for TP-NFPB-COF (Fig. 3c and d and S18, SI). The latter value compares favorably with or exceeds those of several reported porous adsorbents for light hydrocarbon separation, including FJU-36a (2.8),[40] NKCOF-12 (2.3),[19] and USTB-25-3D (2.4)[41] (Table S3, SI). Dynamic breakthrough experiments (50/50, v/v) conducted at a total flow rate of 1.2 mL $min^{-1}$ further demonstrate efficient $C_2H_2/CO_2$ separation by TP-NFPB-COF, with a breakthrough time of 12 min $g^{-1}$, comparable to NKCOF-12 (14 min $g^{-1}$)[19] and FJU-36a (15 min $g^{-1}$)[40] (Fig. S19, SI).

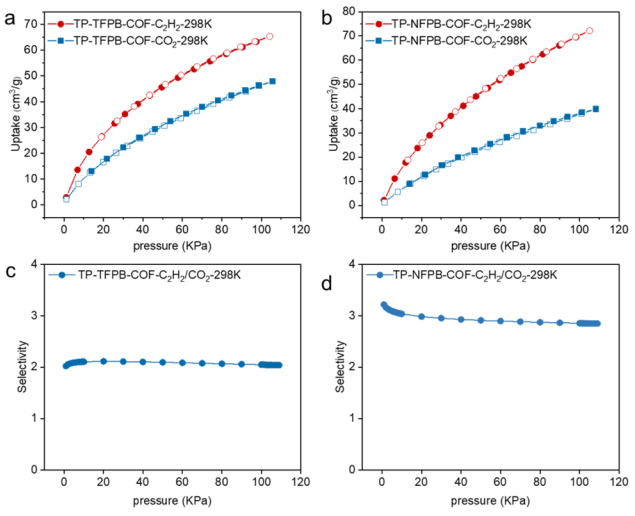


Fig. 3 (a and b) $C_2H_2$ and $CO_2$ adsorption isotherms for (a) TP-TFPB-COF and (b) TP-NFPB-COF at 298 K. (c and d) IAST-predicted selectivities for equimolar $C_2H_2$ and $CO_2$ mixture for (c)TP-TFPB-COF and (d) TP-NFPB-COF at 298 K.

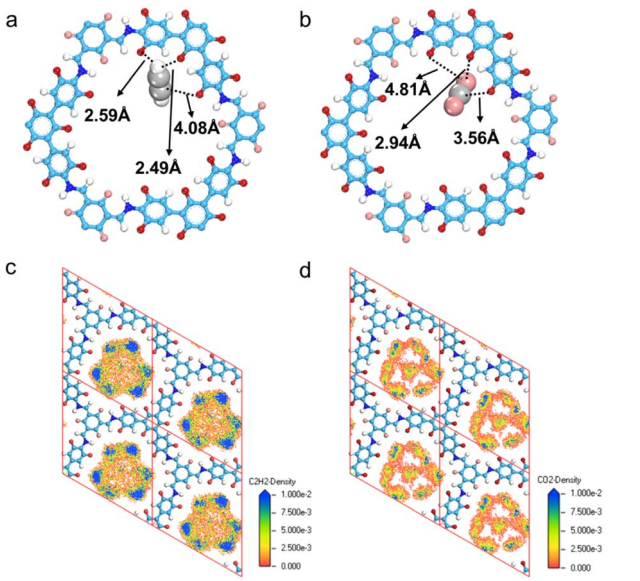


Fig. 4 (a and b) Simulated preferential binding sites of (a) $C_2H_2$ and (b) $CO_2$ in TP-NFPB-COF. (c and d) Guest distribution densities of (c) $C_2H_2$ and (d) $CO_2$ in TP-NFPB-COF, viewed along the *c*-axis.

To elucidate the origin of the enhanced selectivity, grand canonical Monte Carlo (GCMC) simulations were performed to identify preferred adsorption sites of gas molecules within the COF channels (Fig. 4). The simulations indicate that both gases preferentially localize within the hexagonal pore channels. $C_2H_2$ interacts with the framework *via* three C–H···F hydrogen bonds (2.49 Å, 2.59 Å and 4.08 Å; Fig. 4a), whereas $CO_2$ forms three such interactions with longer bond lengths (2.94 Å, 3.56 Å, and 4.81 Å; Fig. 4b), which collectively weaken binding strength. The spatial distribution density maps (Fig. 4c and d) reveal a higher occupancy of $C_2H_2$ around fluorine sites, further corroborating the stronger interaction. These findings demonstrate that the electronegative fluorine moieties within TP-NFPB-COF serve as selective binding sites for $C_2H_2$, thereby enabling efficient discrimination between $C_2H_2$ and $CO_2$ in gas separation applications.

## Conclusions

In summary, two isoreticular two-dimensional COFs with hcb topology were constructed through controlled fluorination, affording frameworks with differentiated fluorine contents and pore microenvironments. Among them, the highly fluorinated TP-NFPB-COF exhibits significantly enhanced $C_2H_2$ uptake and improved $C_2H_2/CO_2$ separation performance relative to TP-TFPB-COF. GCMC simulations reveal that the strengthened selectivity originates from intensified host–guest interactions within the fluorine-rich channels, where electronegative F sites preferentially stabilize $C_2H_2$ molecules. These findings demonstrate that precise fluorine engineering of pore environments represents an effective strategy for modulating gas–framework interactions, offering valuable design principles for COF-based light hydrocarbon separations.

## Author contributions

The individuals listed as authors have contributed to the development of this manuscript, and no other person was involved. The authors' contributions included: L. J. L., W. J. W., and P. Y. H. developed experiments (synthesis and performance test), L. J. L and S. W. carried out the computational research (calculations, analysis, and writing) and literature review, while Y. W. P. developed and composed the original draft, supervised it, and provided sources. All authors have read and agreed to the published version of this manuscript.

## Conflicts of interest

There are no conflicts to declare.

## Data availability

The data supporting the findings of this search are available within the article and its supplementary information (SI). Supplementary information: supporting data for this article are provided in the SI, which includes experimental procedures and characterization data, NMR spectra, and computational and adsorption details. Experimental details, FT-IR, PXRD, SEM, TEM, *etc*. See DOI: https://doi.org/10.1039/d6ra01174h.

## Acknowledgements

Financial support from the National Natural Science Foundation of China (22375179) and the start-up funding from the Pao Yue-kong Leading Talent Program at Ningbo University (ZX2026000104) is gratefully acknowledged.

## Notes and references

1 Y. He, R. Krishna and B. Chen, *Energy Environ. Sci.*, 2012, **5**, 9107–9120.
2 J. Pei, K. Shao, J. X. Wang, H. M. Wen, Y. Yang, Y. Cui, R. Krishna, B. Li and G. Qian, *Adv. Mater.*, 2020, **32**, e1908275.
3 H. Hao, Y. Zhao, D. Chen, J. Yu, K. Tan, S. Ma, Y. Chabal, Z. Zhang, J. Dou, Z. Xiao, G. Day, H. Zhou and T. Lu, *Angew. Chem., Int. Ed.*, 2018, **57**, 16067–16071.
4 X. Zhang, W. Fan, W. Jiang, Y. Li, Y. Wang, M. Fu and D. Sun, *Chem. Eur. J.*, 2021, **27**, 10693–10699.
5 X. Wang, H. Liu, Y. Li, X. Yang, F. Gao, X. Wang, Z. Kang, W. Fan and D. Sun, *Coord. Chem. Rev.*, 2023, **482**, 215093.
6 L. Cai, Z. Yao, S. Lin, M. Wang and G. Guo, *Angew. Chem., Int. Ed.*, 2021, **60**, 18223–18230.
7 B. Li, X. Cui, D. O'Nolan, H. Wen, M. Jiang, R. Krishna, H. Wu, R. Lin, Y. Chen, D. Yuan, H. Xing, W. Zhou, Q. Ren, G. Qian, M. J. Zaworotko and B. Chen, *Adv. Mater.*, 2017, **29**, 18223–18230.
8 M. Zhang, J. Duan, Y. Feng and J. Bai, *Nat. Commun.*, 2025, **16**, 10082.
9 E. Perez-Botella, S. Valencia and F. Rey, *Chem. Rev.*, 2022, **122**, 17647–17695.
10 Z. Xu, X. Xiong, J. Xiong, R. Krishna, L. Li, Y. Fan, F. Luo and B. Chen, *Nat. Commun.*, 2020, **11**, 3163.
11 H. Zeng, M. Xie, Y. Huang, Y. Zhao, X. Xie, J. Bai, M. Wan, R. Krishna, W. Lu and D. Li, *Angew. Chem., Int. Ed.*, 2019, **58**, 8515–8519.
12 L. Zhang, Y. Bao, R. Gao, W. Shi, Y. Guo, L. Hou and Y. Wang, *Chem. Eng. J.*, 2025, **505**, 159641.
13 W. Shi, Y. Li, J. Chen, R. Su, L. Hou, Y. Wang and Z. Zhu, *Chem. Commun.*, 2021, **57**, 12788–12791.
14 G. Singh, J. Lee, A. Karakoti, R. Bahadur, J. Yi, D. Zhao, K. AlBahily and A. Vinu, *Chem. Soc. Rev.*, 2020, **49**, 4360–4404.
15 J. Huang, X. Han, S. Yang, Y. Cao, C. Yuan, Y. Liu, J. Wang and Y. Cui, *J. Am. Chem. Soc.*, 2019, **141**, 8996–9003.
16 N. Huang, X. Chen, R. Krishna and D. Jiang, *Angew. Chem., Int. Ed.*, 2015, **54**, 2986–2990.
17 L. Jiang, Y. Tian, T. Sun, Y. Zhu, H. Ren, X. Zou, Y. Ma, K. R. Meihaus, J. R. Long and G. Zhu, *J. Am. Chem. Soc.*, 2018, **140**, 15724–15730.
18 X. Xiong, L. Zhang, W. Wang, N. Zhu, L. Qin, H. Huang, L. Meng, Y. Xiong, M. Barboiu, D. Fenske, P. Hu and Z. Wei, *ACS Appl. Mater. Interfaces*, 2022, **14**, 32105–32111.

19 P. Zhang, Z. Wang, Y. Yang, S. Wang, T. Wang, J. Liu, P. Cheng, Y. Chen and Z. Zhang, *Sci. China Chem.*, 2022, **65**, 1173–1184.
20 R. Sahoo, S. Mondal, D. Mukherjee and M. C. Das, *Adv. Funct. Mater.*, 2022, **32**, 2207197.
21 R. Sahoo and M. C. Das, *Coord. Chem. Rev.*, 2021, **442**, 213998.
22 L. Chen, C. Gong, X. Wang, F. Dai, M. Huang, X. Wu, C. Lu and Y. Peng, *J. Am. Chem. Soc.*, 2021, **143**, 10243–10249.
23 C. Gong, H. Wang, G. Sheng, X. Wang, X. Xu, J. Wang, X. Miao, Y. Liu, Y. Zhang, F. Dai, L. Chen, N. Li, G. Xu, J. Jia, Y. Zhu and Y. Peng, *Angew. Chem., Int. Ed.*, 2022, **61**, e202204899.
24 Y. Lu, J. He, Y. Chen, H. Wang, Y. Zhao, Y. Han and Y. Ding, *Macromol. Rapid Commun.*, 2018, **39**, 1700468.
25 S. K. Das, X. Wang, M. M. Ostwal, Y. Zhao, Y. Han and Z. Lai, *Chem. Eng. Sci.*, 2016, **145**, 21–30.
26 C. J. Doonan, D. J. Tranchemontagne, T. G. Glover, J. R. Hunt and O. M. Yaghi, *Nat. Chem.*, 2010, **2**, 235–238.
27 Y. Hao, H. Wen, Y. Yu, X. Zhang, Y. Cui, B. Chen, B. Li and G. Qian, *Angew. Chem., Int. Ed.*, 2025, **64**, e202506055.
28 S. Karak, S. Kumar, P. Pachfule and R. Banerjee, *J. Am. Chem. Soc.*, 2018, **140**, 5138–5145.
29 X. Tang, L. Jia, X. Wang, S. Su, Y. Chen, X. Kong, Z. Ye, H. Xie, W. Gong, E. Du, Y. Liu, K. O. Kirlikovali, O. K. Farha and Y. Cui, *Angew. Chem., Int. Ed.*, 2025, **64**, e202424859.
30 Y. Jiang, J. Hu, L. Wang, W. Sun, N. Xu, R. Krishna, S. Duttwyler, X. Cui, H. Xing and Y. Zhang, *Angew. Chem., Int. Ed.*, 2022, **61**, e202200947.
31 L. Liu, Z. Yao, Y. Ye, Y. Yang, Q. Lin, Z. Zhang, M. O'Keeffe and S. Xiang, *J. Am. Chem. Soc.*, 2020, **142**, 9258–9266.
32 P. Tu, X. He, R. Abu-Reziq, C. Pan, J. Tang and G. Yu, *Sep. Purif. Technol.*, 2022, **290**, 120857.
33 J. Liu, G. Zhou, J. Yang, C. Gong, H. Wang, W. Jiao and Y. Peng, *J. Am. Chem. Soc.*, 2025, **147**, 23429–23433.
34 B. Pramanik, R. Sahoo, R. Krishna and M. C. Das, *Small*, 2025, **21**, 2411456.
35 S. K. Das, X. Wang and Z. Lai, *Microporous Mesoporous Mater.*, 2018, **255**, 76–83.
36 J. Li, Z. Cheng, Z. Wang, J. Dong, H. Jiang, W. Wang, X. Zou and G. Zhu, *Angew. Chem., Int. Ed.*, 2023, **62**, e202216675.
37 J. Liu, X. Luo, S. Wang, P. Hao, W. Wei, J. Pan and Y. Peng, *Chem. Commun.*, 2025, **61**, 9492–9495.
38 R. Sanchez-Naya and F. Beuerle, *Angew. Chem., Int. Ed.*, 2025, **64**, e202423676.
39 B. Pramanik, R. Sahoo and M. C. Das, *Coord. Chem. Rev.*, 2023, **493**, 215301.
40 L. Liu, Z. Yao, Y. Ye, L. Chen, Q. Lin, Y. Yang, Z. Zhang and S. Xiang, *Inorg. Chem.*, 2018, **57**, 12961–12968.
41 B. Yu, S. Geng, X. Ding, X. Zhou, Y. Jin, H. Wang, X. Wang, T. Zheng, Z. Zhang and J. Jiang, *Chem*, 2024, **10**, 2170–2179.